AGU PUBLICATIONS

JGR

Journal of Geophysical Research: Space Physics

RESEARCH ARTICLE
10.1002/2017JA024053

**Key Points:**
- Cold plasma blobs in the Jovian plasma sheet show ion composition consistent with physical chemistry models
- Azimuthal flow speeds dip below corotation 9–15 Jovian radii
- Radial profiles of plasma properties are combined to make a 2-D model of plasma sheet

**Correspondence to:**
F. Bagenal,
bagenal@colorado.edu

**Citation:**
Dougherty L. P., K. M. Bodisch, and F. Bagenal (2017), Survey of Voyager plasma science ions at Jupiter: 2. Heavy ions, *J. Geophys. Res. Space Physics*, *122*, doi:10.1002/2017JA024053.

Received 20 FEB 2017
Accepted 28 JUN 2017
Accepted article online 5 JUL 2017

©2017. American Geophysical Union. All Rights Reserved.

# Survey of Voyager plasma science ions at Jupiter: 2. Heavy ions

**L. P. Dougherty[1], K. M. Bodisch[1], and F. Bagenal[1]**

[1]Laboratory for Atmospheric and Space Physics, University of Colorado Boulder, Boulder, Colorado, USA

**Abstract** We take the plasma parameters derived by Bagenal et al. (2017) from Voyager plasma science data in the Jovian magnetosphere and examine the radial profiles of density, temperature, composition, and azimuthal flow. The plasma sheet shows a relatively uniform structure of decreasing electron density ($N_e$) and increasing temperature out to about 20 $R_J$, but beyond about 15 $R_J$ there is increasing disorder with sporadic blobs of cold plasma. These small (~0.5 $R_J$) blobs of cold (~20 eV) plasma make a minor contribution to the net outward flux of iogenic plasma. The ion composition in the cold blobs is consistent with the ion abundances derived from physical chemistry models extending from 6 to ~9 $R_J$, whereupon the collisional reactions slow down and radial transport speeds up, effectively freezing in the ion composition to the following abundances: $O^+/N_e$ = 15–22%, $S^{++}/N_e$ = 10–19%, $O^{++}/N_e$ = 4–8%, $S^{+++}/N_e$ = 4–6%, and $S^+/N_e$ = 1–5%. Beyond about 7 $R_J$ the component of hot (suprathermal, approximately hundreds of eV) ions becomes a significant fraction of the total density. The radial profile of the plasma's azimuthal flow speed shows that corotation begins to breakdown at about 9 $R_J$, dipping down to about 20% below corotation before increasing back up to corotation briefly (~17–20 $R_J$), reaching an asymptotic value of about 225 km/s (corresponding to rigid corotation at ~18 $R_J$). We present a 2-D model of the plasma sheet beyond 6 $R_J$ based on simple functions for the equatorial profiles of plasma properties and steady state diffusive equilibrium along magnetic flux tubes. Cold plasma blobs in the Jovian plasma sheet show ion composition consistent with physical chemistry models. Azimuthal flow speeds dip below corotation 9–15 Jovian radii. Radial profiles of plasma properties are combined to make a 2-D model of plasma sheet.

## 1. Introduction

This paper is the second of three publications surveying the ion data from the Voyager plasma science (PLS) instrument [*Bridge et al*., 1977] at Jupiter. The Voyager PLS ion energy-per-charge (E/*q*) spectra span 10 eV to 6 keV with a resolution of up to ΔE/E ~ 3.6%. *Bagenal et al*. [2017, hereafter Paper 1] describe the PLS instrument, the spacecraft trajectories, and history of previous analyses of these data. In this publication (Paper 2) we address the specific issues of heavy ion composition and plasma sheet structure. The measured abundances of protons ($H^+$) and other minor ions ($Na^+$ and $SO_2^+$) are discussed in *Bodisch et al*. [2017, hereafter called Paper 3].

In March and July of 1979 the Voyager 1 and Voyager 2 spacecraft passed through the Jovian system, approaching at late morning local time, making a closest approach to Jupiter at dusk, then departing in the early morning sector. Voyager 2's closest approach of ~10 $R_J$ (radius of Jupiter = 71,492 km) was outside Europa's orbit, while Voyager 1 reached 4.9 $R_J$, inside the Io torus. The plasma seemed a little hotter on the Voyager 2 pass and the spectral peaks not so distinct. Like previous analyses, we focus on Voyager 1 PLS data.

In analyzing the ion composition, previous analyses of the PLS data [*McNutt et al*., 1981; *Bagenal and Sullivan*, 1981] made assumptions about the plasma (e.g., that the ions had a common temperature or thermal speed, that $O^+$ dominated the composition, or assumed an average ion mass/charge ratio). Analysis of PLS data in the Io plasma torus by *Bagenal* [1985, 1994] and *Bagenal et al*. [1992] was guided by observations of EUV emissions [*Broadfoot et al*., 1979; *Shemansky*, 1987, 1988]. The problem with this latter approach is that knowledge of atomic parameters that quantify emission rates have changed significantly over the nearly four decades since the Voyager flybys (see discussions in *Nerney et al*. [2017]).

Further analysis of Jovian thermal plasma was made by instruments on the Ulysses and Galileo spacecraft. The Ulysses spacecraft used Jupiter for a gravity assist out of the ecliptic plane and used its solar wind instruments for measuring the plasma environment in the magnetosphere. Initial observations of ion composition

in the 600 eV to 60 keV range are reported by *Geiss et al*. [1992], but only counts were reported for different species and not absolute densities or abundances. As far as we know, quantitative comparison with other measurements has not been reported. The Galileo mission was severely hampered by the loss of its main antenna, and the data were severely decimated. *Bagenal et al*. [2016] present a survey of the Galileo PLS data in the Jovian plasma sheet, but the low spectral resolution and data decimation did not allow detailed determination of ion composition.

At higher energies (30 keV–150 MeV) ion abundances in the Jovian magnetosphere have been determined by the Voyager Low Energy Charged Particle instrument [*Krimigis et al*., 1981; *Hamilton et al*., 1981; *Mauk et al*., 1996] and Cosmic Ray Spectrometer [*Vogt et al*., 1979a, 1979b]. Further measurements of these energetic (~0.2–10 MeV/n) ion populations were made with the Galileo Energetic Particle Detector instrument [*Maclennan et al*., 2001; *Mauk et al*., 2001; *Clark et al*., 2016]. Ulysses detected energetic (~0.6–1.6 MeV/n) $H_3^+$ ions from Jupiter's atmosphere [*Lanzerotti et al*., 1993] which we will discuss further, in relation to the thermal proton population measured by Voyager PLS, in Paper 3.

While these measurements of high-energy heavy ion composition in the magnetosphere of Jupiter are very important (the suprathermal populations dominate the particle pressure which exceeds the local magnetic field pressure by up to 2 orders of magnitude), it is not clear how they relate to the thermal heavy ion population observed by Voyager PLS in the torus and plasma sheet. It seems likely that the ultimate source of sulfur and oxygen ions is the volcanic $SO_2$ gases from Io. But how the torus plasma is accelerated to MeV energies remains unknown. Moreover, the acceleration processes probably depend on the mass and/or charge of the ion being accelerated. A major advantage of the instruments on the Juno mission [*Bagenal et al*., 2014] is a substantial overlap in the energy of particles that they detect which will allow careful characterization of the suprathermal populations and their relationship to the thermal populations.

In this paper we take the output of fitting Voyager PLS ion spectra presented in Paper 1 and use these measurements to develop an empirical model of the heavy ion plasma in Jupiter's plasma sheet. In section 2 we summarize the method of analyzing the PLS spectra. In section 3 we present radial profiles of the local parameters derived from fits: density and temperature, ion composition, and azimuthal flow speed. In section 4 we discuss the isolated regions ("blobs") of cold plasma. Section 5 discusses how we map the plasma densities along magnetic field lines to derive empirical functions for the radial distribution of plasma properties along the centrifugal equator and to construct 2-D maps in radial distance and latitude. Finally, section 6 presents our conclusions.

## 2. Deriving Plasma Properties From PLS Data

Paper 1 describes the method used to fit the Voyager PLS ion energy-per-charge (E/*q*) spectra (spanning 10 eV to 6 keV) with convected Maxwellian functions for each ion species. Different assumptions were made in the fitting processes, depending on how well resolved the spectral peaks are for the various ion species and how many of the four PLS sensors have significant signal. A key parameter controlling how well composition can be determined is the Mach number of the flow, i.e., the ratio of bulk flow speed to thermal speed. When the plasma is cold (low thermal speed), the comoving ion species are well separated in E/*q* with a narrow thermal spread around a well-resolved spectral peak. For example, in the very high Mach flows of the cold inner torus the ion composition and all three components of the plasma bulk flow (assuming that all ion species are comoving with the same bulk flow) were allowed to vary as fit parameters. In regions where the plasma was transonic or even subsonic, we had to assume the abundances of the different ion species and fix the bulk speed to a fraction of rigid corotation with Jupiter. In the middle magnetosphere (12–40 $R_J$) the Voyager spacecraft encountered isolated regions where the plasma was considerably colder than the surroundings ("cold blobs"), where the composition and flow could be well constrained.

### 2.1. Composition

In the region between ~6 and 8 $R_J$ the Io plasma torus glows in bright UV emission lines of the different ions of sulfur and oxygen. These multiple line emissions were first detected by the ultraviolet spectrometer (UVS) instrument on Voyager 1 (then 6 months later Voyager 2) as the spacecraft approached Jupiter [*Broadfoot et al*., 1979; *Sandel et al*., 1979]. During its Jupiter gravity-assist flyby en route to Saturn, the Cassini spacecraft took high-resolution spectral observations with the Ultraviolet Imaging Spectrometer

**Table 1.** Heavy Ion Composition From Physical Chemistry Model of *Delamere et al*. [2005][a]

| | At 6 $R_J$ | At 9 $R_J$ |
|---|---|---|
| $O^+/N_e$ | 28% | 20% |
| $O^{++}/N_e$ | 3% | 7.5% |
| $S^+/N_e$ | 7% | 3% |
| $S^{++}/N_e$ | 20% | 17% |
| $S^{+++}/N_e$ | 2.5% | 7% |
| O/S | 1.05 | 1.02 |
| <M > (amu) | 23.8 | 23.9 |
| <Z> | 1.5 | 1.7 |

[a]Assumes ~10% of the total charge density is contributed by protons.

[*Esposito et al*., 2004] for 6 months between 1 October 2000 and 31 March 2001. By analyzing the ~90 emission lines spanning from 561 Å in the EUV to 1913 Å in the FUV observed by the Cassini Ultraviolet Imaging Spectrometer (UVIS), *Steffl et al*. [2004a, 2004b, 2006] determined the torus properties (electron temperature and ion abundances) over space (radial distance and longitude) and time.

How do the Voyager PLS data relate to the Cassini UV observations obtained 22 years later? In particular, analysis of the Cassini UVIS measurements reported by *Steffl et al*. [2004a, 2004b] suggested a very different ion composition in the torus to that present based on Voyager UVS by *Shemansky* [1987]. The problem is that analysis of UV emissions depends heavily on atomic data from lab studies for emission and reaction rates, and these "constants" have varied enormously over the past decades. *Nerney et al*. [2017] present a review of UV studies of the Io plasma torus and reanalyzes Voyager, Galileo, and Cassini data using the CHIANTI 8.0 data base [*Dere et al*., 1997]. They found that they could match the Voyager (1979) UVS data with more or less the same composition as derived from the higher-resolution Cassini (2000) UVIS data.

Another approach is to look at physical chemistry models of the Io plasma torus. *Delamere and Bagenal* [2003] developed a physical chemistry code that takes a source of neutral atoms (O and S) and a radial transport rate, calculates the reactions (ionization, charge exchange, and radiation), and solves equations of conservation of mass and energy. It has been known for many years that to match the observed UV emissions and ion composition, additional energy needs to be provided via a source of hot (suprathermal) electrons [*Barbosa and Moreno*, 1988; *Shemansky*, 1988]. *Delamere and Bagenal* [2003] added parameters (the temperature of a hot electron population and their fraction of the total electron density) to their model required to match the Cassini UVIS observations. *Delamere et al*. [2005] used a radial version of the physical chemistry model to match the *Steffl et al*. [2004b] radial ion emission profile and derived ion abundances plus electron properties (density, temperature, and hot electron population) that require a neutral cloud ejected from Io at a rate of 0.7–1.2 t $s^{-1}$ with O/S ~ 2, consistent with dissociation of $SO_2$ from Io's volcanoes.

*Delamere et al*. [2004] modeled the factor ~2 decline in emission reported by *Steffl et al*. [2004a] with an approximately month-long outburst, corresponding to a factor ~3 increase in neutral production by Io in the August before the Cassini flyby. *Steffl et al*. [2008] showed that variations with longitude (both System III and System IV) could be modeled by modulating the fraction of hot (suprathermal) electrons. Before invoking temporal and spatial variations in composition, however, we start with a standard composition based on a steady state model. We conclude, therefore, that the place to start in reanalyzing the Voyager PLS ion data is the radial profile of ion composition derived from a physical chemistry model by *Delamere et al*. [2005] to match the Cassini UVIS observations reported by *Steffl et al*. [2004a, 2004b].

In our analysis of the Voyager PLS ion data, when the spectral peaks are not distinct, we constrain the composition of the plasma by using the *Delamere et al*. [2005] values for the density of $O^{++}$, $S^+$, $S^{++}$, and $S^{+++}$ ions as ratios of the $O^+$ ion density (Table 1). Beyond 9 $R_J$ it was assumed that the density of the plasma became tenuous enough to halt further chemical reactions. We extrapolated the ion composition from 9 $R_J$ outward, with little change from the outer edge of the torus model. In most cases we show (Paper 1, Figure 3) that this standard composition fits the cold, resolved spectra very well. But in certain cases in the plasma sheet, the standard composition did not match up and we made minor adjustments to the composition to produce a better fit to the data.

### 2.2. Ion Temperatures and Hot Component

On ionization, a fresh ion picks up a gyrospeed equal to the local plasma flow speed (close to rigid corotation in the Io torus). Given the amount of Coulomb coupling in the torus, one might expect the pickup ions to

have evolved from a pickup ring beam to a Maxwellian distribution and the temperatures to be close to isotropic. Indeed, the Galileo PLS instrument (that covered a much larger field of view than Voyager PLS) indicated isotropic distributions in the Io torus [*Crary et al*., 1998]. Energy flows from ion pickup toward equilibration (via Coulomb interactions) between the ions and to the electrons (which also cool via exciting UV ion emissions). Models show that over the tens of days the ions spend in the torus they cool to temperatures well below their corotational pickup energies (270 eV for $O^+$ and 540 eV for $S^+$). *Delemere et al*. [2005] estimated that at ~6 $R_J$ the $S^{++}$ and $O^+$ ions reach a similar temperature of ~90 eV. The higher-ionization states ($S^{+++}$ and $O^{++}$) cool a little further (~75 eV), while the $S^+$ ions remain hotter (~150 eV).

In the cold, inner torus the well-resolved peaks allow the separate ion temperatures to be determined and demonstrates that inside Io's orbit the high densities and long residence times have produced a plasma where all the ions share a common temperature except for a small population (few percent abundance) of suprathermal ions. Where the plasma is warmer and the spectral peaks merge together, we fit the spectra with a fixed composition and allow a common (isotropic) temperature to vary. Since the composition is dominated by the M/Q ~ 16 species and the abundance of $S^+$ drops to a few percent, we keep things simple and give all of the species the same temperature. Specifying the $S^+$ temperature to be the same as the M/Q = 16 species provides an upper limit to the amount of $S^+$ ions. Furthermore, in the outer torus to plasma sheet region the small population of $S^+$ ions overlaps in energy with the increasing population of suprathermal ions.

In the cold torus, where ion temperatures range between 1 and 10 eV, it was evident that a hotter ion species is also present, with a temperature around 100 eV. Using the same convected Maxwellian model, it was possible to match this hot component of the plasma distribution using a single hot $O^+$ ion population. In reality, this hot population of the plasma is likely a superposition of multiple ion species. Outside the cold torus the suprathermal tail to ion spectra had less shape and likely more consistent with a power law or Kappa function that extends above the 6 keV range of the PLS instrument. Fitting this suprathermal tail with Maxwellian $O^+$ ions is clearly a crude approximation. In future studies, the PLS data could be combined with the higher-energy Voyager Low Energy Charged Particle data [*Krimigis et al*., 1981] and a Kappa distribution applied to determine the suprathermal tails of the distributions. On the other hand, the Juno data will soon provide a better coverage of the suprathermal tail to the ion distributions.

### 2.3. Cases

Paper 1 describes (and illustrates with examples) the five types of circumstances (cases i to v) that were used to fit the spectra: (1) case i (blue)—variation of all parameters (mostly in the inner cold torus); (2) case ii (red)—constraining the ion abundances of the five main ion species (O+, O++, S+, S++, and S+++) to the standard composition based on *Delamere et al*. [2005] as listed in Table 1; (3) case iii (black)—fixed ion composition plus fixed flow speed; (4) case iv (green)—cold blobs in the plasma sheet where resolved peaks can be fit allowing some variation in composition; and (5) case v (purple)—interpolation between the composition of the cold torus and the standard composition at 6 $R_J$ from *Delamere et al*. [2005].

The colors (in parentheses) correspond to the bars at the bottom (Voyager 1) of Figures 1 and 2 and top (Voyager 2) of Figure 1.

## 3. Local Plasma Properties

In Paper 1 the plasma parameters derived from fitting the Voyager PLS ion spectra are plotted (Figures 4 and 5) versus time for the two flybys (with uncertainties in each fit parameter) and compared with previous analyses [*McNutt et al*., 1981; *Bagenal and Sullivan*, 1981; *Bagenal*, 1985] in Figure 6. The densities and temperatures derived in our reanalysis are similar to those from earlier studies. In this paper we concentrate on the heavy ions, their composition, and investigate their spatial variation. For clarity we have not included the uncertainties in each parameter on the plots in this paper. Figures 4 and 5 of Paper 1 show the uncertainties in the determination of plasma parameters to be on the order of a percent in the cold torus, rising to ~20% in the plasma sheet, particularly where the plasma is hot ($T > 100$ eV).

### 3.1. Density and Temperature

In Figure 1 we have combined the measurements from both Voyager spacecraft to show the charge density and the temperature of the heavy ions as a function of radius for Voyager 1 in March 1979 (inbound data in

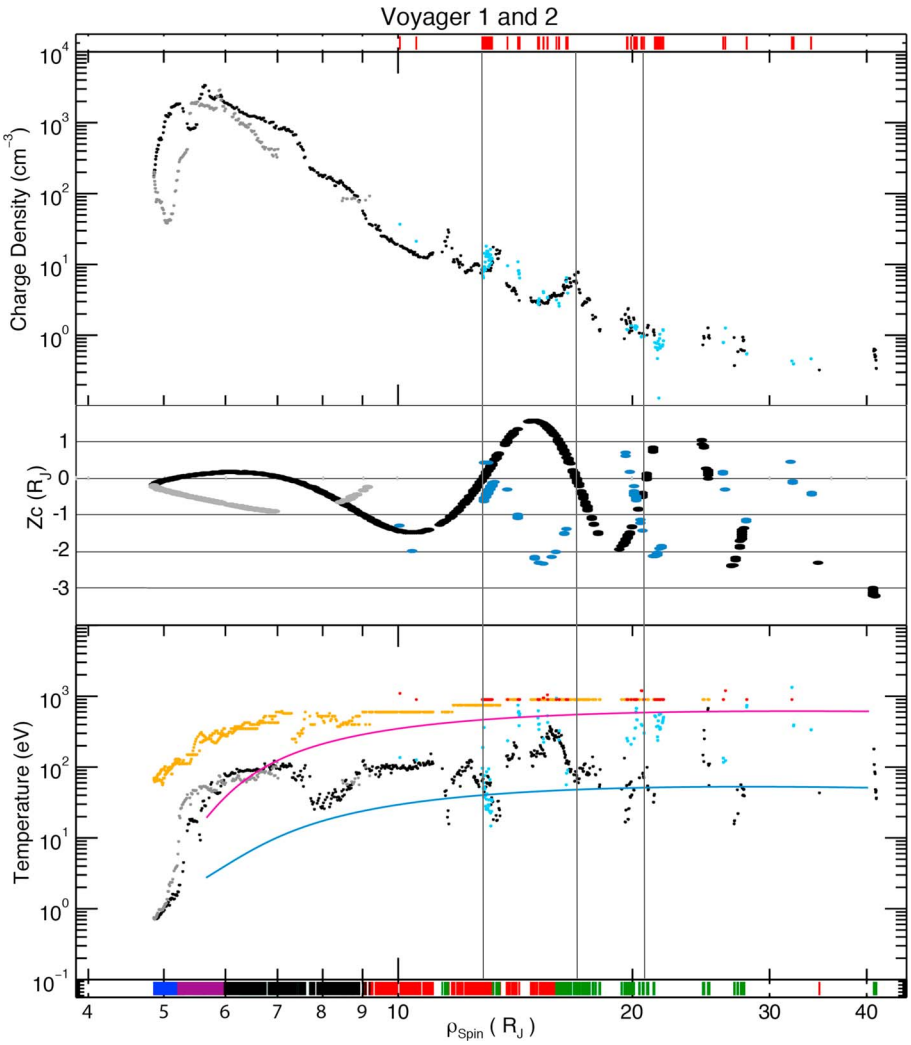


**Figure 1.** Radial profiles of in situ (top) density and (bottom) temperature from Voyager 1 (inbound black and outbound gray) and Voyager 2 (blue). (middle) The vertical distance ($Z_C$) of the spacecraft from the centrifugal equator. The different ways of fitting the ion data are shown for each point along the bottom/top strip for Voyager 1/2. Case i is blue, case ii is red, case iii is black, case iv is green, and case v is purple. Figure 1 (bottom), the yellow (Voyager 1) and red (Voyager 2) dots are the temperatures of the suprathermal component and the blue and magenta lines show the thermal and suprathermal electron temperatures derived by *Sittler and Strobel* [1987].

black and outbound in gray) and Voyager 2 in July 1979 (blue points). These plasma properties vary with distance ($Z_C$) from the centrifugal equator (the farthest point along the magnetic field line from Jupiter's spin axis). The $Z_C$ of the spacecraft is plotted in the middle panel of Figure 1. The confinement of the plasma to the centrifugal equator is illustrated by comparing the inbound (black) data obtained when the spacecraft was close to the centrifugal equator with the outbound (gray) points obtained well below the equator, particularly in the cold inner torus where the density scale height is very small (~0.1 $R_J$). In the plasma sheet (>10 $R_J$) the plasma tends to be colder and denser near the equator (the three vertical gray lines are where Voyager 1 crossed the centrifugal equator at 13, 17, and 21 $R_J$). Beyond ~20 $R_J$ the geometry of the plasma sheet can be quite irregular with increasing departures from a planer, centrifugally confined sheet with distance from Jupiter, as first shown by *McNutt et al.* [1981].

In Figure 1 (bottom), the temperature of the suprathermal component (assumed to be $O^+$) is shown with yellow dots for Voyager 1 and red for Voyager 2. The parameter constraints (i.e., cases i to v) used in the fits are illustrated by colored vertical lines below (Voyager 1) and above (Voyager 2). The boundary between the cold inner torus and warm outer torus is at ~5.7 $R_J$, well inside Io's orbital distance (5.9 $R_J$). The ion

temperature (assumed common to all heavy ions) in the 6–9 $R_J$ region is comparable to the $T$(M/Q = 16) temperature derived in the *Delamere et al*. [2005] physical chemistry model.

For comparison with the temperature of the heavy ions, we show profiles of the electron temperature based on *Scudder et al*. [1981] and *Sittler and Strobel* [1987] analyses of Voyager 1 PLS electron data. In the outer, warm torus the electrons are heated via Coulomb collisions with the heavy ions that pick up corotational energy (270 eV for $O^+$ and 540 eV for $S^+$) on ionization. But this energy is quickly radiated away via electron impact excited UV emissions [*Delamere and Bagenal*, 2003], leaving the thermal electron population (blue curve) about a factor ~20 colder than the torus heavy ions. *Sittler and Strobel* [1987] found that the suprathermal tail to the electron distribution (magenta curve) was small in the main torus (<1%) but increased to >10% beyond about 10 $R_J$. Inside ~5.5 $R_J$ the flux of electrons with energy above the 10 eV threshold of the PLS instrument drops below the detectable limit. Extrapolating the blue curve inward indicates that the electrons thermally equilibrate with the ions inside ~5.3 $R_J$, consistent with the high densities and expected long residence times in the cold torus.

The ion temperature in the plasma sheet was generally warmer for the second flyby with Voyager 2 (blue dots) having a tendency for slightly higher temperatures than Voyager 1 (shown in black) beyond ~12 $R_J$, with fewer occasions of cold, dense blobs. This general tendency for density and temperature to be anticorrelated was found by *Bagenal et al*. [2015] in a survey of plasma conditions at Europa's orbit (9.4 $R_J$) from the Galileo PLS data.

Modulation of UV emissions in the torus with longitude [*Sandel and Dessler*, 1988; *Volwerk*, 1997; *Volwerk et al*., 1997; *Herbert and Sandel*, 2000; *Steffl et al*., 2006] was followed up with studies of the extensive Galileo PLS data by *Frank and Paterson* [2000a, 2000b, 2004] and *Frank et al*. [2002] who found higher temperatures in the longitude region of 267–295°. Further examination of ion temperatures from all Galileo orbits by *Bagenal et al*. [2016] suggests, however, that any System III variations in ion temperature are transitory on timescales of weeks. The limited longitudinal coverage by the Voyager flybys restricts our ability to address temperature versus longitude here.

### 3.2. Ion Composition

Figure 2 shows the composition of the individual heavy ions in the magnetosphere as measured by Voyager 1 (the higher temperatures on the Voyager 2 pass produced broad ion spectra where the separate species could not be resolved which meant we needed to assume the standard ion composition). Figure 2 (first and second panels) shows the two prevalent oxygen species, and Figure 2 (third to fifth panels) show the three sulfur species that appear in the PLS data. The relative abundances of these five species are shown as the ratio of each density divided by the total charge density of just these five heavy ion species. In each case, the values corresponding to the *Delamere et al*. [2005] composition for >9 $R_J$ are shown as horizontal black lines. Figure 2 (sixth panel) shows the ratio of the suprathermal component (assumed to be $O^+$) relative to the total charge density of all ion species which comprised at times as much as 40% of the total charge density. Again, the strips at the bottom show colored bars indicating the case type used in fitting the spectra.

In the region of 6–9 $R_J$ the separate spectral peaks of the different ion species are merged into a single broad peak (see examples shown in Figures 3b and 3c in Paper 1) and the relative abundances of the main ion species are fixed to that of the *Delamere et al*. [2005] physical chemistry model. Outside this region, the composition was first assumed to follow *Delamere et al*. [2005] and then adjusted by hand to better match the data. In the outer plasma sheet there are times when the plasma flow moved the $S^+$ spectral peak above the 6 keV threshold of the PLS instrument. In other places, the density of $S^+$ dipped too low to produce a measureable signal. As illustrated in Paper 1 with sample spectra, there are occasions where the plasma was sufficiently cold to show distinct spectral peaks for the different ion species (Figures 3a and 3d of Paper 1). In some of these cold blobs the composition deviated noticeably (up to a factor of 2 in abundance) from the *Delamere et al*. [2005] composition. For example, at ~12 $R_J$ the abundance of $S^+$ increased while $S^{+++}$ decreased. The opposite effect (increase in average charge state) is shown at ~17 $R_J$ with both $S^{+++}/S^+$ and $O^{++}/O^+$ increasing. Such modulation of the $S^+/S^{+++}$ abundance ratio is similarly observed in the Io torus UV emissions and was shown by *Steffl et al*. [2006] to be consistent with just a minor modification of the fraction of hot electrons. We suggest that these cold blobs exited the torus (and collisions ceased) at a time (several days before the Voyager flyby) when the fraction of hot electrons was atypical.

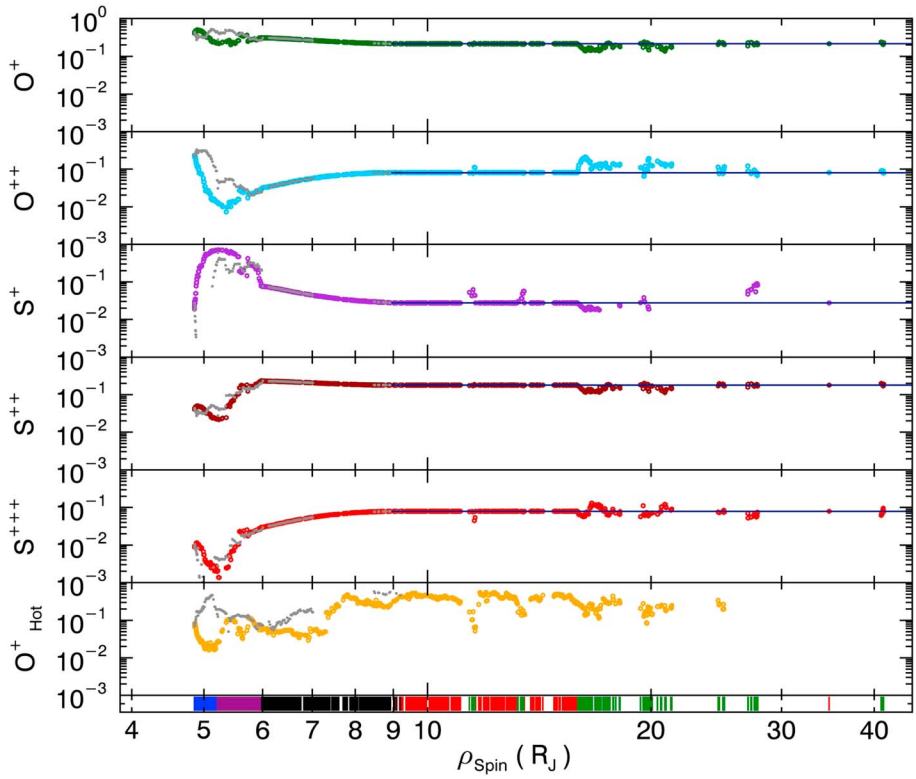


**Figure 2.** (first to fifth panels) Radial profiles of ion abundances from Voyager 1 (colors inbound and gray outbound) where in each of the first to fifth panels the local ion density has been divided by the sum of the charge density of just these ion species (excluding protons and minor ions). (sixth panel) The density of the suprathermal ions divided by the total charge density. In the bottom strip the colored vertical bars show where the different case types were used to fit the spectra (same as Figure 1).

In the cold, inner torus (inside ~5.7 $R_J$) the composition changes quite dramatically. Earlier analyses [*Bagenal et al*., 1980; *Bagenal and Sullivan*, 1981; *Bagenal*, 1985] only considered the Voyager 1 inbound data where the flow was directly into all three main sensors and the cold beam response could be applied. In this reanalysis (where we are using the *Barnett and Olbert* [1986] instrument response) we are able to extend the analysis outbound where the spacecraft passed well below the centrifugal equator, the densities dropped and the corotational flow was more oblique into the main sensors.

As Voyager 1 passed inbound inside ~5.7 $R_J$ (remaining very close to the centrifugal equator) the temperature plummeted, the average charge state of the ion species decreased, and the overall charge (electron) density decreased. At Jupiter, for a single species (atomic mass $A_i$ amu), plasma of temperature $T_i$ (in eV) in a dipole field, the density ($N_i$) decreases with height ($Z_C$ in Jovian radius) from the centrifugal equator as.

$$N_i(Z_C) = N_i(0)\exp - (Z_C/H)^2$$

where the scale height is $H(R_J) = 0.64\ (T_i/A_i)^{1/2}$ [*Bagenal*, 1994]. Thus, as the ion temperature drops from 80 eV at ~6 $R_J$ to 10 eV at ~5.5 $R_J$ to 1 eV at ~5.1 $R_J$, the scale height for $S^+$ (the dominant ion in the cold torus) drops from 1 $R_J$ to 0.4 $R_J$ to 0.1 $R_J$. This means that in the cold inner torus the plasma is very tightly confined to the centrifugal equator and the sharp drop in $S^+$ abundance shown in Figure 2 inside ~5.1 $R_J$ is due to the spacecraft moving just a fraction of a Jovian radius from the centrifugal equator. Extrapolating local measurements to the centrifugal equator and integrating along the field line then becomes extremely sensitive to both knowledge of the spacecraft trajectory and the field geometry. *Bagenal* [1994] showed that inside ~5.3 $R_J$ the difference in $Z_C/H$ for the spacecraft derived from different field models increases significantly and any extrapolation along the field line becomes unreliable.

In the cold, inner torus, where temperatures drop below 1 eV, one would not expect there to be significant abundance of ions at multiple ionization states. Yet the spectra clearly show $O^{++}$ (and, to a lesser extent,

$S^{+++}$) rising inward of ~5.3 $R_J$ and remaining high on the outbound leg where the spacecraft moved away from the centrifugal equator. *Bagenal and Sullivan* [1981] showed that when a full, multispecies description is derived for the distribution along the field line (see Appendix A), the density of minor high-ionization state ions peaks off the equator. Similarly, the density of $O_{hot}^{+}$ is also higher outbound, consistent with less confinement to the equator. *Brown et al*. [1983] pointed out that the recombination rates are very slow in the torus so that the higher-ionization state ions are only removed via charge exchange. The electrostatic force of the ambipolar electric field pulls the $O^{++}$ and $S^{+++}$ ions off the equator, limiting the opportunities for charge exchange with $S^{+}$.

By analyzing the change in slope of the total flux tube content at ~5.7 $R_J$, *Richardson et al*. [1980] concluded that the radial transport of plasma inward of this distance was a few percent of the total outward flux and at a speed of about a factor of 50–100 times slower than the azimuthal flow, presumably because centrifugally driven flux tube interchange favors outward transport of mass. This slow inward transport suggests that the plasma in the cold torus has been there for months. On the other hand, when trying to model profiles of flux tube content and ion temperature with radial diffusion models, *Richardson and Siscoe* [1983] found it difficult to reproduce the profiles with source confined to Io's orbit, even when including drastic time variability (though see *Bagenal* [1985] for discussion of implications of later ion temperature correction). *Herbert et al*. [2008] revisited ground-based observations of $S^{+}$ emissions from the early 1990s and constructed a simple model of plasma slowly diffusing inward from the "ribbon" region (extending 5.9–6.1 $R_J$ radially, ~1 $R_J$ vertically) to the "washer" shape region that extends 5.0–5.6 $R_J$ (varying with longitude) but just 0.2 $R_J$ in vertical width. They assumed the plasma started with warm torus composition based on *Bagenal* [1994] and found that to sustain the observed bright optical $S^{+}$ emission in both the ribbon and washer regions they needed to add a substantial source of energy to power the emissions and keep the ions warm enough to maintain the vertical extent of even the thin washer.

The PLS spectra around 5.2 ± 0.2 $R_J$ (e.g., Figure 3a in Paper 1) clearly show $SO_2^{+}$ ions and a hot, suprathermal population of ions which we model as $O^{+}$ but could be other recently picked up species. The presence of these species indicates that the cold torus plasma does not entirely come from ionization close to Io that has simply convected inward and that there are sources (and possibly sinks) inward of Io's orbit. Ground-based observations of $S^{+}$ emissions from the cold torus indicate significant variations with Io phase, System III longitude and local time, and Io's volcanic activity (see reviews by *Thomas et al*. [2004], *Schneider and Bagenal* [2007], and *Herbert et al*. [2008]). A fully 3-D, time-variable model of the physical chemistry of Io's neutral cloud and inner torus is needed to explore the complicated structure of this small region of plasma inside Io's orbit. After multiple passes of the Juno spacecraft close to Jupiter we expect that a more accurate model of the magnetic field, necessary for accurately locating the centrifugal equator, will be developed [*Connerney et al*., 2017].

### 3.3. Azimuthal Ion Flow

Figure 3 shows the azimuthal flow speed from our reanalysis of PLS data. The plasma in the Io plasma torus is coupled by Jupiter's strong magnetic field to the planet's ionosphere. Jupiter's spin period is 9 h 55 m 29.711 s = 9.92492 h. At a cylindrical distance from the spin axis of $\rho_{spin}$ (in Jovian radius) the corotation speed is 12.57 × $\rho_{spin}$ km/s. Figure 3 (top) shows the ratio of the locally measured azimuthal speed to corotation.

In the cold torus (<5.6 $R_J$) the plasma is clearly very close to rigid corotation [*Bagenal*, 1985]. The few cases of supercorotation shown in Figure 3 (top) are from the Voyager 1 outbound pass when there were issues with a change in orientation of the spacecraft that moved the direction of corotation away from the fields of view of the PLS sensors. We suggest that these few points do not indicate significant supercorotation. In the warm torus (6–7 $R_J$) the broad, overlapping peaks in the spectra do not allow a determination of the flow speed better than within ~10% of corotation. Ground-based spectral emissions $S^{+}$ ions suggest a dip in the corotation curve of 4% at 6 $R_J$ (presumably due to ion pickup near Io's orbit), returning to corotation outward by 7 $R_J$ and inward in the cold torus [*Brown*, 1994; *Thomas et al*., 2001].

Outside the Io torus, between 7 and 9 $R_J$, the spectra show few features and while strict corotation and standard composition [from *Delamere et al*., 2005] do not match the spectrum very well, we found that modifying the speed, the protons or the hot ion population could each produce reasonable matches to the data. So we maintained standard composition and allowed the azimuthal speed to drop to 95% of

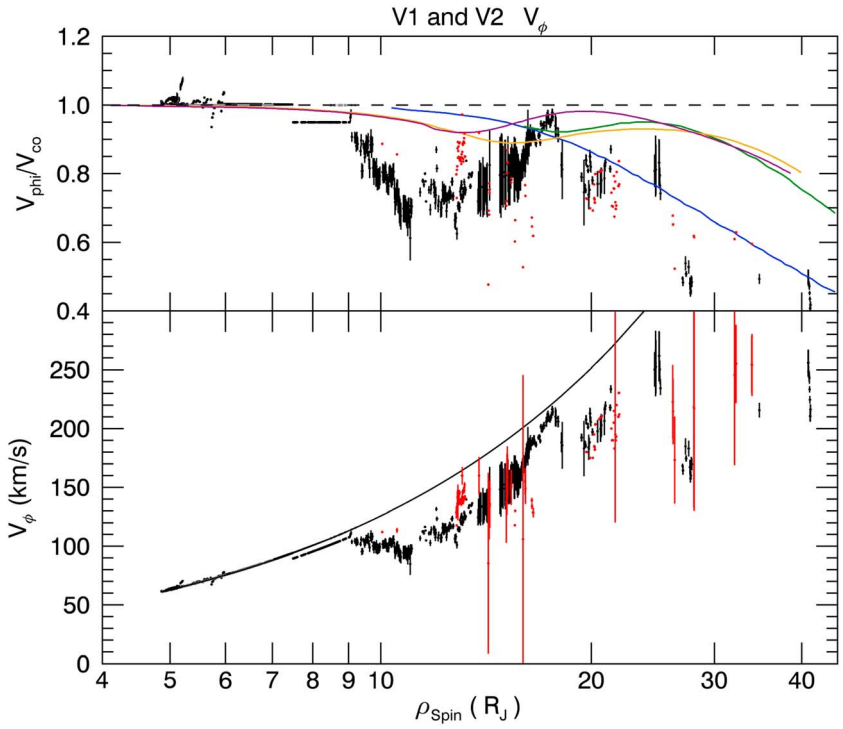


**Figure 3.** (bottom) Radial profile of azimuthal flow speed from Voyager 1 (black) and Voyager 2 (red) with uncertainties derived from the fit to the spectra (see Paper 1). (top) The locally observed speeds (with the large error bars for the red Voyager 2 points removed for clarity) were divided by the local corotation speed and compared with theoretical models of *Hill* [1980] (blue), *Nichols and Cowley* [2004] (yellow), *Ray et al.* [2010] (green), and *Smith and Aylward* [2009] (purple). Between 6 and 9 $R_J$ the fits were case iii (see black bars in Figure 1) which means that the flow speeds were fixed to rigid corotation (or a fraction thereof) so no error bars are shown.

corotation (but we fully admit that this is somewhat ad hoc and the true uncertainties in flow, composition, and temperature are substantial in this region).

Figure 3 shows the first significant break from rigid corotation appears around 9–10 $R_J$ as the plasma slows down briefly but is then sped back up toward corotation around 17 $R_J$. An example of a spectrum with distinct spectral peaks from this region of corotation lag is shown in Paper 1 Figure 3d at 13.364 $R_J$ where the azimuthal speed is 79% of corotation. Beyond ~20 $R_J$, corotation breaks down and the plasma azimuthal flow remains at speeds typically around 225 km/s out to the farthest distance (~42 $R_J$) where the Voyager PLS instrument was able to make good measurements. This asymptotic value of 225 km/s corresponds to rigid corotation at ~18 $R_J$. Note that the plasma flow can only be well determined when the ion temperature is cold enough to produce resolved peaks which tends to happen in transient cold regions and it is not clear if these cold blobs are typical of the ambient plasma sheet.

As the plasma diffuses radially outward (due to centrifugally driven flux tube interchange) additional angular momentum must be added to the plasma to keep it corotating [*Hill*, 1979]. At some point the coupling to the ionosphere breaks down and the plasma bulk speed begins to deviate from strict corotation. *Hill* [1980] matched the azimuthal flow speed profile from early analysis of the Voyager PLS data by *McNutt et al.* [1979] and concluded that the deviation of corotation from about ~20 $R_J$ outward was consistent with a plasma production rate of $10^{30}$ amu $s^{-1}$ (1700 kg/s) and an ionospheric conductance of ~0.1 mho. Note that the *McNutt et al.* [1979] profile matches the profile in Figure 3 but only comprised Voyager 1 data from 11.5 to 22.5 $R_J$ including just a couple points in the inner couple Jovian radii.

Figure 3 (top) shows the ratio of the measured azimuthal flow to the speed of corotation. We have compared this corotation fraction with the theoretical models (colored curves). The blue curve shows the flow profile where the plasma production is 1000 kg/s and corotation is limited by the electrical conductivity of Jupiter's ionosphere (assumed to be 0.1 mho) as originally derived by *Hill* [1980]. The orange and green

curves show the effects of two additional factors: (a-orange) enhanced ionospheric Pederson conductivity due to precipitating electrons in the auroral regions [*Nichols and Cowley*, 2004] and (b-green) also including a Pederson conductance enhanced by precipitation (but different functional form) and adding a parallel electric field at high latitudes where low electron density limits the flow of currents between the planet and the plasma sheet [*Ray et al*., 2010, 2012]. The primary motive of introducing a localized electric field is to accelerate electrons across the potential (~30–200 kV) [*Gustin et al*., 2004] into Jupiter's atmosphere where they excite the main auroral emissions. A secondary consequence (supplementing the effect of precipitation-enhanced Pederson conductance) is that the electrical currents are increased at the equator and the plasma is accelerated back toward corotation after the initial lag.

One approach to addressing this magnetosphere-ionosphere-thermosphere (M-I-T) coupling is to say that decoupling between the thermosphere and ionosphere reduces (by about a half) the effective Pederson conductance [*Huang and Hill*, 1989; *Pontius*, 1995; *Pontius et al*., 1998; *Nichols and Cowley*, 2004]. Other models address M-I-T coupling self-consistently [*Smith and Aylward*, 2009; *Ray et al*., 2015] with the thermospheric flows responding (via collisions) to supercorotational flows in the ionosphere that arise in response to the momentum transfer to the magnetosphere. The purple curve in Figure 3 is from *Smith and Aylward* [2009] for a mass-loading rate of 1000 kg/s and a background Pederson conductance reduced to 0.01375 mho.

While the shape of the purple and green curves are consistent with the data, the deviation from corotation needs to be stronger and initiate much closer in. This suggests that either the plasma production must be much higher than 1000 kg/s or the ionospheric conductance reduced. Constrained by UV emissions in the torus, *Delamere and Bagenal* [2003] derived a plasma source based on their physical chemistry model of the Io torus of 800 kg/s for the Voyager 1 epoch and 1400 kg/s for Voyager 2. Such constraints on the plasma source suggest that Jupiter's ionospheric conductance would need to be significantly reduced to produce the deviation from corotation indicated in Figure 3. Or there is something missing from the models that would produce subcorotation closer to Jupiter.

The plasma flow is primarily in the azimuthal direction, but, on some occasions, there are noticeable components in the radial and/or vertical directions needed to match the data. In particular, around ~5 $R_J$ in the cold torus where the high Mach number of the flow allowed a good measure of the flow vector, there were sometimes vertical components of up to 3 km/s. These small perturbations of the flow are less than 5% of the background azimuthal flow. During the Voyager 2 flyby, there was a large compressional event, forcing an inward radial component of the velocity (~50 km/s). The nonazimuthal flows were explored extensively by *McNutt et al*. [1981] and by *Sands and McNutt* [1988] who argued for the plasma motion being mostly field aligned and driven by solar wind compression and expansion of the magnetosphere.

## 4. Cold Blobs

In Figure 1 there are several regions of the plasma where the temperature dips below the general 100 eV temperature of the plasma sheet. In these regions of colder plasma, the spectral peaks are more resolved. These cold blobs stand out in the overview spectrograms of Voyager PLS data in Paper 1 (Figure 2a) which also shows examples of the fitted spectra (Figure 3d). While *McNutt et al*. [1981] noted regions of cold plasma where the flow could be quantified, they did not quantify the properties of such regions.

In Figure 4 of this paper we show the evolution of one of these cold blobs (the farthest blob, at 41.2 $R_J$) as the spacecraft flew through it. The only measured signal was in the D Faraday cup due to the spacecraft orientation in this region, so we are not able to derive the full flow vector but the flow is consistent with 42% of corotation. The plasma gradually changes over the 28 min duration with the temperature increasing from 37 eV to 180 eV as the density ranges from 0.34 to 0.62 $cm^{-3}$ (average 0.51 ± 0.1 $cm^{-3}$). The composition does not vary much throughout the blob with $O^+/N_e$ = 22 ± 1%, $S^{++}/N_e$ = 19 ± 1%, $O^{++}/N_e$ = 8.5 ± 0.5%, and $S^{+++}/N_e$ = 7.4 ± .8% which is pretty similar to the composition of *Delamere et al*. [2005] shown in Table 1.

On the Voyager 1 inbound pass we see about nine blobs of cold material over about 37 h when the spacecraft moved from 42 to 11 $R_J$. They each last about 20–50 min during which the spacecraft moved about 0.2–0.9 $R_J$. We cannot accurately evaluate from the PLS spectra what the density contrast is inside versus outside the blobs because when the plasma is hotter and the signal spread across many energy

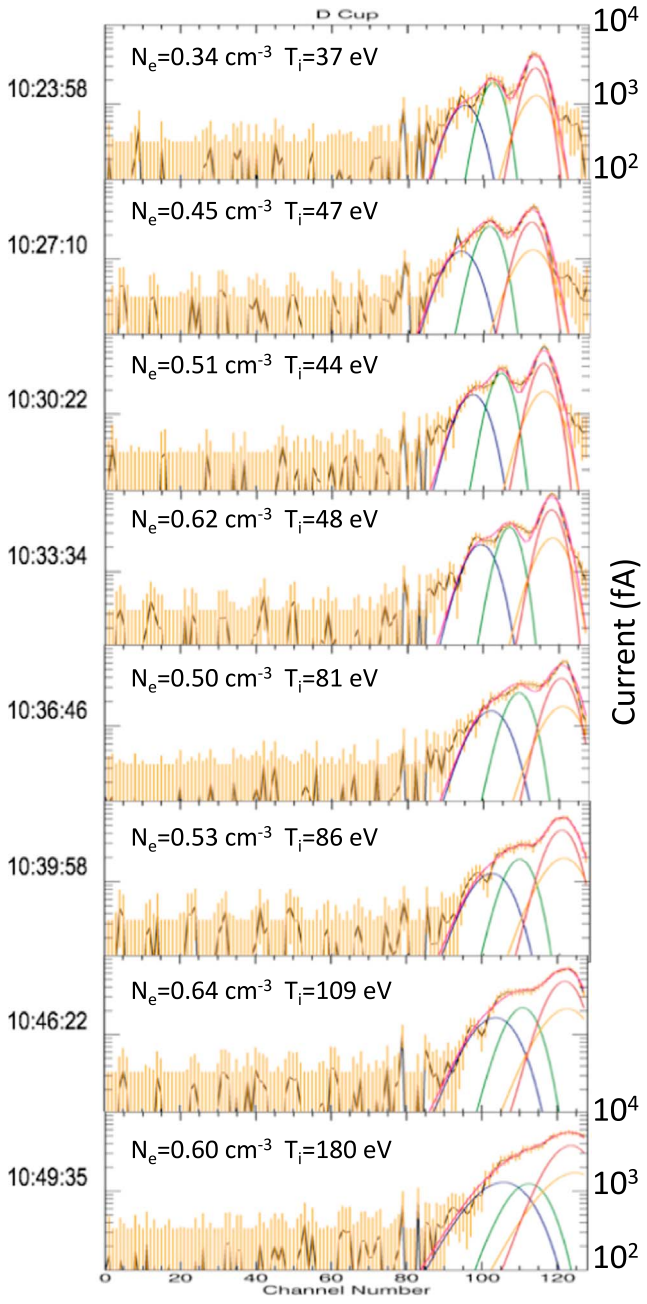


**Figure 4.** Series of eight spectra in a cold blob observed by Voyager 1 at 41.2 $R_J$. The time on day of year 62 (3 March) 1979 of each observation is shown to the left of each spectrum. The data are shown with black lines (units of femto amperes) with measurement errors shown in orange. Fits to the data comprise contributions from $O^+$ (brown), $S^{++}$ (orange), $S^{+++}$ (green), and $O^{++}$ (blue), adding up to a total simulated current in red. The total charge density and common ion temperature are shown for each fitted spectrum. The channel numbers correspond to 128 energy-per-charge steps, logarithmically spaced between 10 eV and 6 keV with a resolution of $\Delta E/E \sim 3.6\%$..

channels it is hard to determine the density. Analysis of Voyager plasma wave data by *Barnhart et al.* [2009] shows a similar density of 0.5 cm$^{-3}$ at this time with a density about 5 times lower in the surrounding region (Figure 6 of Paper 1). The example shown in Figure 4 has the ion temperature dropping to 37 eV. In some of the blobs the temperature drops below 20 eV (see Figure 1). Some of these cold blobs occur near the centrifugal equator (Figure 1), but several occur well away from the equator.

If we take the typical timescale of ~30 min to correspond to an ~0.5 $R_J$ (quasi-static) size, then each blob is just 0.3% of the circumference of the plasma sheet (at a typical distance of 20 $R_J$). We make a rough estimate of the total mass of each blob to be about 1000 kg which is a minute fraction of the total mass of the plasma disk. If we take a typical timescale for radial transport of ~50 days, then to account for the ~500 kg/s of plasma transported out of the Io plasma torus [*Bagenal and Delamere*, 2011], there would need to be 2 million such 1000 kg cold blobs per 50 days. In the 37 h Voyager 1 took to pass from 42 to 11 $R_J$ this translates into a total of 62,000 cold blobs that would be transported outward, which implies that Voyager would have passed through nearly 200 of blobs for the cold blobs to account for all of the mass transport from the torus. The observation of just nine cold blobs in 37 h indicates that these cold regions are not the primary means of outward transport.

Before Voyager, radial transport via flux tube interchange was thought to be driven by turbulent motions in the atmosphere and ionosphere [*Siscoe and Chen*, 1977; *Siscoe*, 1978]. With the Voyager discovery of the dense warm torus and plasma sheet (compared with the small volume of the cold inner torus) it was clear that outward transport had to be faster than inward [*Richardson et al.*, 1980; *Siscoe and Summers*, 1981]. *Summers and Siscoe* [1985, 1986] described this asymmetric diffusive transport as centrifugally driven flux tube interchange. *Pontius et al.* [1986] pointed out the need for the inward transport of flux tubes carrying low density of plasma but

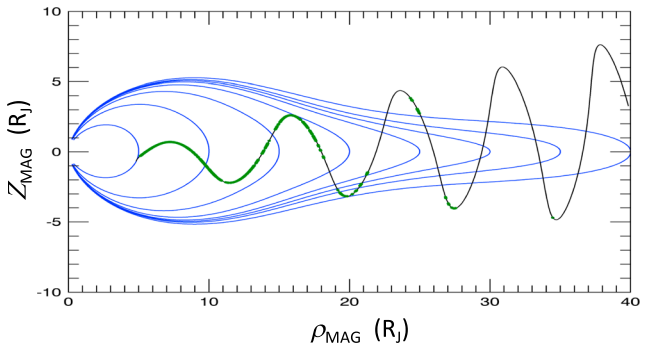


**Figure 5.** The Voyager 1 inbound trajectory is shown in magnetic dipole coordinates where the *Z* axis is pointed along the tilted dipole direction (tilted 9.5° toward System III longitude of 201°) and the *X* axis is the cylindrical distance ($\rho_{MAG}$ in Jovian radius) from the dipole axis. The blue curves are magnetic field lines corresponding to the VIP4 internal field [*Connerney et al*. 1998] plus the CAN current sheet model [*Connerney et al*. 1981].

returning the necessary magnetic flux to maintain steady state. These early descriptions were basically fluid in scale. Others argued for transport on a kinetic scale. Specifically, *Abe and Nishida* [1986] suggested that the transport happens on the scale of the ion gyroradius, while *McNutt et al*. [1987] argued that beyond the torus, where the plasma heats up in the plasma sheet, pressure anisotropy could drive ballooning mode instabilities.

To address the issue of the spatial scale of radial transport processes, *Richardson and McNutt* [1987] analyzed the Voyager PLS data between 6 and 11 $R_J$ to look for variations in ion fluxes at the highest temporal measurement cadence. They were able to put a limit on the scale of density perturbations of less than 10% on spatial scales down to 20 km. This ruled out the models of *Pontius et al*. [1986] and *Summers and Siscoe* [1985] who postulated the interchange of relatively empty and full flux tubes under the assumption that the density per magnetic flux remains constant. But the low-contrast flux tube interchange observed by *Richardson and McNutt* [1987] may be limited to the dense torus region. It is clear from Figure 1 that beyond ~10 $R_J$ the plasma becomes much more variable, not only from the occurrence of occasional coherent cold blobs but also from the overall variability of density and temperature. Such variability beyond ~10 $R_J$ is confirmed by plasma data from the Ulysses flyby [*Phillips et al*., 1993] and the multiple orbits by Galileo [*Bagenal et al*., 2015, 2016].

There are two likely reasons that the Galileo PLS instrument was not able to detect distinct volumes of cold plasma similar to the cold blobs we report here from the Voyager PLS data: (1) due to the malfunction of the Galileo antenna, the PLS data were heavily decimated except in priority regions around the moons; and (2) the Galileo PLS instrument has a lower energy resolution so that it was not able to resolve the separate spectral peaks that allowed us to identify the cold blobs in the Voyager PLS data. A survey of the Galileo PLS data is presented in *Bagenal et al*. [2016].

Small regions of inward moving, low-density flux tubes have been best identified via enhancements of the magnetic field strength [*Kivelson et al*., 1997], whistler emission [*Bolton et al*., 1997], and energetic particle fluxes [*Thorne et al*., 1997] in the Io plasma torus (6–8 $R_J$). *Kivelson et al*. [1997] reported 15 events lasting ~0.5–5 min corresponding to sizes as small as 1000 km to 0.3 $R_J$. *Russell et al*. [2005] showed a survey of ~30 enhancement events in the Galileo magnetometer data and argued that these were flux tubes likely depleted of thermal plasma, returning magnetic flux to the torus. *Mauk et al*. [1999] presented a survey of >100 events over the Galileo mission where energetic particles were injected over larger time periods (approximately in hours) between 9 and 27 $R_J$.

While there are plenty of models [*Vasyliunas*, 1989; *Fazakerley and Southwood*, 1992, 1993; *Yang et al*., 1992, 1994; *Pontius et al*., 1998; *Kivelson and Southwood*, 2005] suggesting scales (ranging from a few kilometers to a Jovian radius) for interchanging flux tubes carrying dense, thermal plasma, and magnetic flux outward and more rapid injection of smaller flux tubes bringing in energetic particles and returning magnetic flux, the observational evidence of such spatial scales at the tens to hundreds of eV energies of thermal plasma remains sparse. The cold blobs of plasma observed by Voyager 1 between 11 and 42 $R_J$ are part of the process but not the whole story.

## 5. Two-Dimensional Model

To extrapolate the Voyager PLS measurements to the equator, we need to calculate how plasma is distributed along the magnetic field. In Appendix A we show the procedure, based on diffusive equilibrium in a

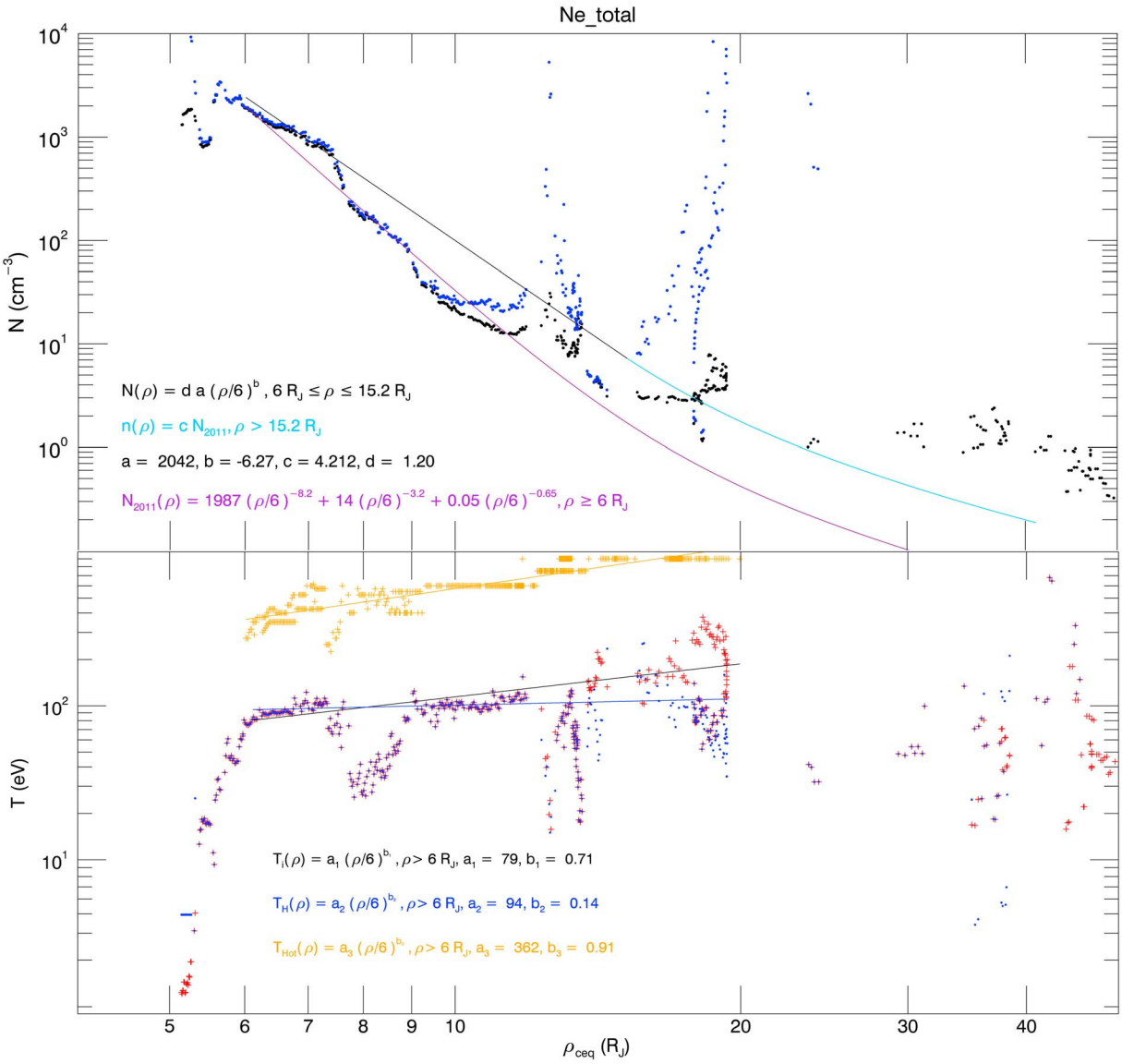


**Figure 6.** (top) Radial profile of electron density with an empirical power law fit between 6 and 15.2 $R_J$ (black curve). The power law function derived by *Bagenal and Delamere* (2011) from Galileo and Voyager data is shown in purple. Beyond 15.2 $R_J$ this 2011 curve has been scaled up (blue) to meet the black curve. (bottom) Radial profiles of temperatures of (black) heavy ions, (blue) protons, (yellow) suprathermal ions. Constants for the power law functions are shown in Tables 2 and 3.

rotating magnetic field [*Bagenal*, 1994]. We use a magnetic field model that combines the internal sources of the VIP4 model of *Connerney et al*. [1998] plus the field associated with an azimuthally symmetric equatorial current from *Connerney et al*. [1981], which we call VIP4 + CAN (Figure 5). We trace the magnetic field from the location of the spacecraft at the time of each measurement and find the centrifugal equator—the location farthest from Jupiter's spin axis. We then take the local measurements and extrapolate the plasma properties to the centrifugal equator.

Figure 5 shows how the magnetic field geometry changes from close to dipolar (<10 $R_J$) to highly stretch out due to azimuthal currents in the equatorial plasma disk. The Voyager 1 trajectory is shown in tilted dipole coordinates to illustrate how the spacecraft remains pretty close to the magnetic equator within ~15 $R_J$. Beyond ~15 $R_J$, the combined effect of the 9.5° tilt of the magnetic field and the stretching of the field lines due to azimuthal currents means that when the spacecraft is not close to the magnetic equator, it is connected to field lines that extend to very large radial distances. Furthermore, as illustrated in Figure 1, the plasma properties become increasingly disorganized. This means that it becomes increasingly hard to extrapolate from the spacecraft along magnetic field lines to the centrifugal (or magnetic) equator.

**Table 2.** Power Law Functions for Density Profiles at the Centrifugal Equator Beyond 6 $R_J$[a]

| Species | $N_i/N_e(6\ R_J)$ | $a$ | $b$ | $c$ |
|---|---|---|---|---|
| $e^-$ | 1 | 2451 | −6.27 | 4.21 |
| $O^+$ | 24% | 592 | −7.36 | 0.368 |
| $O^{++}$ | 3% | 76.3 | −6.73 | 0.086 |
| $S^+$ | 7% | 163 | −6.81 | 0.169 |
| $S^{++}$ | 22% | 538 | −6.74 | 0.598 |
| $S^{+++}$ | 4% | 90.7 | −6.21 | 0.165 |
| $H^+$ | 2% | 50.6 | −5.31 | 0.212 |
| $Na^+$ | 4% | 97.2 | −6.75 | 0.106 |
| $O^+_{hot}$ | 6% | 134 | −4.63 | 1.057 |
| B&D 2011 | | $n_{2011}(R) = 1987\ (R/6)^{-8.2} + 14\ (R/6)^{-3.2} + 0.05\ (R/6)^{-0.65}$ | | |
| $6 \le R \le 15.2$ | | $n(R) = a\ (R/6)^b$ | | |
| $R > 15.2$ | | $n(R) = c\ n_{2011}(R)$ | | |

[a]All densities are in units of $cm^{-3}$. B&D 2011 refers to the electron density profile of *Bagenal and Delamere* [2011].

Figure 1 shows the location of the Voyager 1 and 2 with respect to the centrifugal equator at the time of the measurements we used in this study. Beyond about 15 $R_J$ and above a couple Jovian radii away from the centrifugal equator or when the spacecraft moved through a cold blob, the extrapolation becomes less reliable as the equatorial current sheet stretches out the magnetic field. Between 5 and 6 $R_J$ we use the locally measured quantities from the inbound pass extrapolated to the centrifugal equator because of the spacecraft's close proximity to the equator for this region (Figure 1).

Figure 6 shows profiles of the local electron density (black dots) and extrapolated to the centrifugal equator (blue dots) using the diffusive equilibrium model for the distribution of the plasma along the field line. For these density values extrapolated to the centrifugal equator, an empirical power law function has been created as a function of the radial distance along the centrifugal equator (black line). Parameters for the empirical radial profiles of density for all species are shown in Table 2. An empirical formula for electron density based on a combination of Voyager and Galileo data from *Bagenal and Delamere* [2011] is shown as a purple line. As the extrapolation of Voyager data to the equator becomes less reliable beyond ~15 $R_J$, we have scaled up the *Bagenal and Delamere* [2011] profile beyond 15.2 $R_J$ (light blue curve).

In Figure 6 (bottom) we have plotted radial profiles of ion temperature of the heavy ions (black), protons (blue), and suprathermal population (yellow) versus distance in the centrifugal equator (assuming that there is no change in temperature along the magnetic field). Table 3 gives the power law parameters for these ion temperature radial profiles and electron temperature profiles based on *Scudder et al.* [1981] and *Sittler and Strobel* [1987]. Inside 6 $R_J$ we used the values of these plasma properties extrapolated to the centrifugal equator. As discussed in section 3.2 above, the extrapolation is fine when the spacecraft is close to the centrifugal equator (7 to 5.2 $R_J$), but inside ~5 $R_J$ the scale height of the cold plasma is so small that extrapolation is very sensitive to the magnetic field model applied.

At two longitudes (System III = 110.8° and 290.8°) the jovigraphic, magnetic, and centrifugal equators align. We picked these longitudes and used the above empirical functions of density, temperature, and flow speed to derive two-dimensional maps of the plasma in the $\rho_{centrifugal} - Z_{centrifugal}$ plane. Figure 7 shows maps (top to bottom) of density for total charge, $O^+$, $O^{++}$, $S^+$, $S^{++}$, $S^{+++}$, and $O_{hot}^+$. The maps have been truncated at 5 $R_J$ radial distance and latitude of 35°. As expected, the latitudinal distribution of the density N of $S^+$ is particularly tightly confined to the equator and the plasma sheet density of lighter, hotter, and higher-ionization species are more spread vertically. The hot population is essentially uniform along the field line (since the thermal energy exceeds the

**Table 3.** Power Law Functions for Radial Profiles of Temperature Beyond 6 $R_J$[a]

| | $a$ | $b$ |
|---|---|---|
| $T_{ion}(R) = a\ (R/6)^b$ | 79.3 | 0.714 |
| $T_{proton}(R) = a\ (R/6)^b$ | 94.1 | 0.14 |
| $T_{hot}(R) = a\ (R/6)^b$ | 362 | 0.91 |
| $T_e(R) = a\ (R/6)^b R > 12\ T_e = 50$ eV | 4.6 | 3.4 |
| $T_{ehot}(R) = a\ (R/6)^b R > 12\ T_{ehot} = 600$ eV | 35 | 4.2 |
| $N_{hot}/N_{cold} = a\ (R/6)^b R > 11\ N_{hot}/N_{cold} = 0.1$ | 0.001 | 8 |

[a]All temperatures are in units of eV. $T_{ion}$ refers to all ions except protons and the hot component.

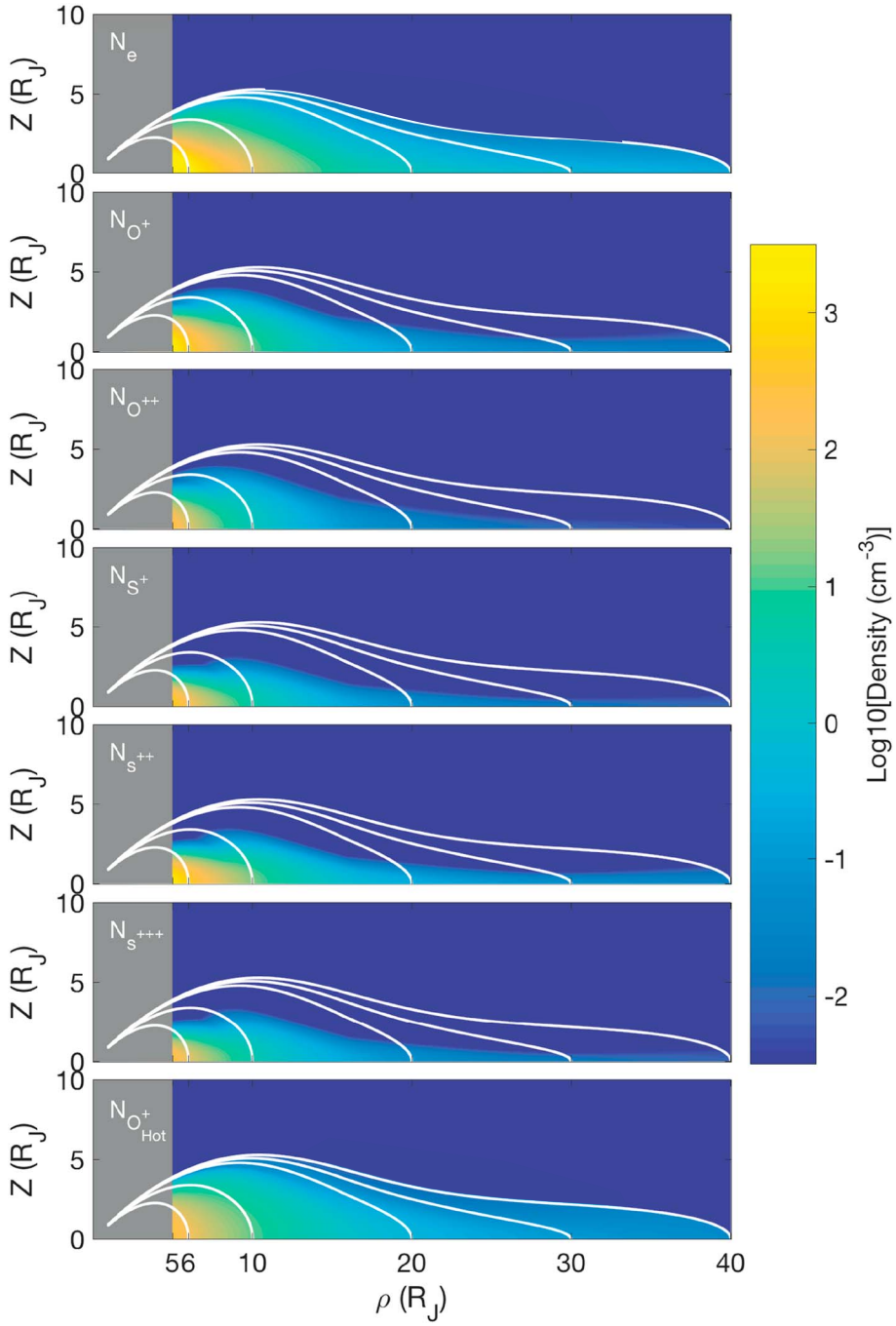


**Figure 7.** Distribution of net charge and different ion species in the plane of distances along and above the centrifugal equator at the System III longitudes where the rotation and magnetic equators align.

corotational energy) and extends beyond the 35° cutoff of our plot. We expect that the plasma sheet density distribution will be much better quantified after the Juno mission.

## 6. Conclusions

Analysis of Voyager PLS ion data in the Jovian system leads us to the following conclusions:

1. The plasma sheet shows a relatively uniform structure of decreasing density and increasing temperature out to about 20 $R_J$, but beyond about 15 $R_J$ there is increasing disorder with sporadic

blobs of cold plasma. Beyond about 7 $R_J$ the fraction of hot (hundreds of eV) ions increases to over 50% beyond ~8 $R_J$.

2. The ion composition in the cold blobs is consistent with the ion abundances derived from physical chemistry models extending from 6 to ~9 $R_J$ where the collisional reactions slow down and radial transport speeds up, effectively freezing in the ion composition to the following abundances: $O^+/N_e$ = 15–22%, $S^{++}/N_e$ = 10–19%, $O^{++}/N_e$ = 4–8%, and $S^{+++}/N_e$ = 4–6%, $S^+/Ne$ = 1–5% which is pretty similar to the composition derived by *Delamere et al*. [2005] based on Cassini UVIS observations.
3. The radial profile of the plasma's azimuthal flow speed shows that corotation begins to breakdown at about 9 $R_J$, dipping down to about 20% below corotation before increasing back up to corotation briefly (~17–20 $R_J$) before decreasing to constant values of about 225 km/s (corresponding to rigid corotation at ~18 $R_J$). This dip and temporary return to corotation is similar in nature to the profiles produced by theoretical models [*Huang and Hill*, 1989; *Pontius*, 1995; *Pontius et al*., 1998; *Nichols and Cowley*, 2004; *Smith and Aylward*, 2009; *Ray et al*., 2010, 2014, 2015], but the observed corotation breakdown at ~9 $R_J$ is much closer in than the theories predict. This perhaps suggests that the ionospheric conductance is weaker than the values assumed in these models or that there is additional decoupling of the plasma sheet from the ionosphere.
4. The presence of small (~0.5 $R_J$) blobs of cold (~20 eV) plasma is intriguing—partly because they provide high-quality spectra that allow good determination of composition—but they comprise a small fraction of the total mass of the plasma sheet and make a minor contribution to the net outward flux of iogenic plasma.
5. We present a 2-D model of the plasma sheet beyond 6 $R_J$ based on simple functions for the equatorial profiles of plasma properties and steady state diffusive equilibrium along magnetic flux tubes.

In Paper 3 of the sequence we discuss the abundances of protons and other minor ions ($H^+$, $Na^+$, and $SO_2^+$) derived from analysis of the Voyager PLS ion spectra.

## Appendix A: Appendix: Diffusive Equilibrium Along the Magnetic Field

To derive the steady state distribution of plasma along a magnetic field line, we start with the equation of force balance (neglecting gravity):

$$(\nabla \cdot P)_{\parallel} + N_i\, m_i \left(\frac{dV}{dt}\right)_{\parallel} + N_i\, Z_i\, q\, E_{\parallel} + N_i \frac{d}{dS}\left[\frac{GM_J\, m_i}{r}\right] = 0 \tag{A1}$$

Figure A1 illustrates the geometry. The first term, the parallel pressure gradient, consists of two terms

$$\frac{dP_{\parallel}}{dS} - (P_{\parallel} - P_{\perp})\frac{1}{B}\frac{dB}{dS} \tag{A2}$$

where the second term is zero for an isotropic plasma ($T_{\perp} = T_{\parallel}$) but if there is a significant thermal anisotropy (A= $T_{\perp}/T_{\parallel}>1$) then a larger fraction of particles have pitch angles closer to perpendicular and therefore tend to be near the magnetic equator. A significant thermal anisotropy has the effect of concentrating the plasma toward the magnetic equator. In steady state conditions the second term in equation (A1) is the centrifugal force:

$$N_i\, m_i \left(\frac{dV}{dt}\right)_{\parallel} = -N_i\, m_i\, q\, \frac{\partial}{\partial S}\left(\frac{1}{2}\Omega^2\rho^2\right) \tag{A3}$$

where $\Omega$ is the spin rate (adjusted for any subcorotation) and $\rho$ is the cylindrical distance from Jupiter's spin axis. The third term in (A1) is the ambipolar electric force:

$$N_i Z_i q E_{\parallel} = N_i Z_i q\, \frac{\partial \phi}{\partial S} \tag{A4}$$

where $\phi$ is the electric potential. Thus, equation (A1) becomes

$$\frac{\partial P_{\parallel}}{\partial S} - (P_{\parallel} - P_{\perp})\frac{1}{B}\frac{dB}{dS} - N\, m_i\, q\, \frac{\partial}{\partial S}\left(\frac{1}{2}\Omega^2\rho^2\right) + N_i Z_i q\, \frac{\partial \phi}{\partial S} = 0 \tag{A5}$$

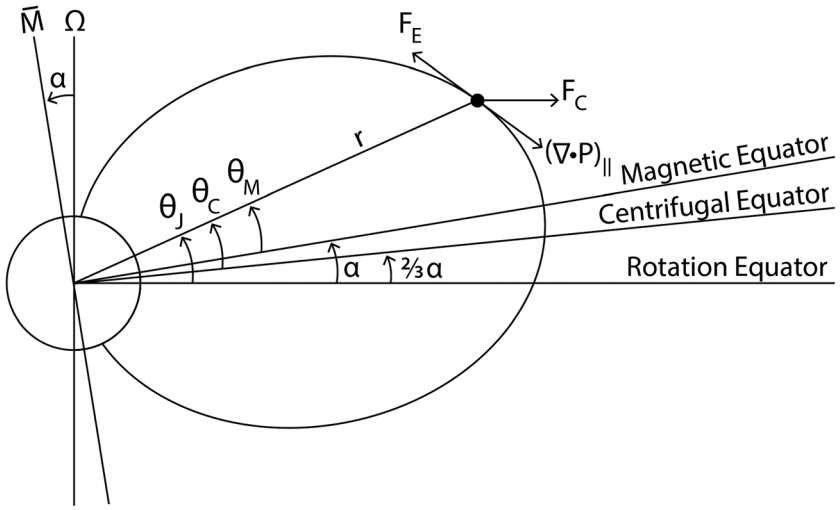


**Figure A1.** Geometry of a dipolar magnetic field where the dipole ($M$) is tilted by an angle ($\alpha$) from the planet's spin axis ($\Omega$). At a position ($r$, $\theta_J$) the components of the directions of the local centrifugal, ambipolar, and pressure gradient forces are shown. The peak density is found at the centrifugal equator, the farthest point from the spin axis along the magnetic field.

If we assume $P_{\parallel} = N_i T_{\parallel}$ (where $T$ is in eV) and $T_{\parallel}$ is constant along the field line, then

$$\frac{1}{N_i}\frac{\partial N_i}{\partial S} = \frac{(T_{\parallel} - T_{\perp})}{T_{\parallel}}\frac{1}{B}\frac{dB}{dS} + \frac{m_i}{T_{\parallel}}\frac{\partial}{\partial S}\left(\frac{1}{2}\Omega^2\rho^2\right) - N_i Z_i q\frac{\partial \phi}{\partial S} \tag{A6}$$

or

$$\frac{\partial}{\partial S}\log N_i = \frac{\partial}{\partial S}\left[\left(1 - \frac{T_{\perp}}{T_{\parallel}}\right)\log B + \frac{1/2\, m_i\, \Omega^2\rho^2}{T_{\parallel}} - \frac{Z_i q\phi}{T_{\parallel}}\right] \tag{A7}$$

Integrating along the field line from a reference point $S_o$ to $S$, we have

$$N_i(S) = N_i(S_o)\exp\left[\left(1 - \frac{T_{\perp}}{T_{\parallel}}\right)\log\frac{B(S)}{B(S_o)} + 1/2\, m_i\, \Omega^2\left\{\frac{\rho^2(S) - (\rho^2(S_o)\}}{T_{\parallel}} - \frac{Z_i q\{\phi(S) - \phi(S_o)\}}{T_{\parallel}}\right]\right. \tag{A8}$$

This gives us $N$ equations, one for each ion and electron species. We set $\phi(S_o) = 0$ (since we are only interested in ambipolar potential relative to our reference location $S_o$). Closing the set of equations by imposing local charge neutrality $N_e = \sum Z_i N_i$ , we have $N + 1$ equations and unknowns so we can solve for $N_i(S)$ and $\phi(S)$. This means that for any location along the field we have a set of inputs: reference densities $n_i(S_o)$, temperatures $T_i$ and anisotropies $A_i$, geometry ($S$ and $\rho$), and magnetic field (specifically, $\{\log B(S)/B(S_o)\}$). The outputs are $N_i(S)$ and $\phi(S)$. For an isotropic plasma (as assumed in this paper), $A_i = 1$ and the first term inside the square brackets is zero. At one $e$-fold drop in $N_i$, approximately a scale height off the equator, $Zi\ q\ \phi(S)$ is comparable to the ion temperature and the ambipolar potential ranges from ~1 V in the cold torus to 100 V in the plasma sheet.

**Acknowledgments**
The authors thank John Belcher and John Richardson for their assistance in accessing the PLS and trajectory data and with translation of the original analysis code. The diligent archiving of PLS documentation by Ralph McNutt is gratefully appreciated. We thank Robert Wilson, Frank Crary, and Licia Ray for useful discussions. The raw Voyager PLS data are archived in the Planetary Data System (PDS—https://pds.nasa.gov/). We have gathered the data for the Jovian magnetosphere, the fitting routines, and the output of our analysis and comparisons with previous analyses of these PLS data at Jupiter here: http://lasp.colorado.edu/home/mop/missions/voyager. We acknowledge support from NASA's Jupiter Data Analysis Program (NNX09AE03G) and the Juno mission (SWRI subcontract 699050X).

## References

Abe, T., and A. Nishida (1986), Anomalous outward diffusion and associated heating of iogenic ions in the Jovian magnetosphere, *J. Geophys. Res.*, *91*, 10,003–10,011, doi:10.1029/JA091iA09p10003.

Bagenal, F. (1994), Empirical model of the Io plasma torus: Voyager measurements, *J. Geophys. Res.*, *99*, 11,043–11,062, doi:10.1029/93JA02908.

Bagenal, F. (1985), Plasma conditions inside Io's orbit: Voyager measurements, *J. Geophys. Res.*, *90*, 311–324, doi:10.1029/JA090iA01p00311.

Bagenal, F., and P. A. Delamere (2011), Flow of mass and energy in the magnetospheres of Jupiter and Saturn, *J. Geophys. Res.*, *116*, A05209, doi:10.1029/2010JA016294.

Bagenal, F., and J. D. Sullivan (1981), Direct plasma measurements in the Io torus and inner magnetosphere of Jupiter, *J. Geophys. Res.*, *86*, 8447–8466, doi:10.1029/JA086iA10p08447.

Bagenal, F., J. D. Sullivan, and G. L. Siscoe (1980), Spatial distribution of plasma in the Io torus, *Geophys. Res. Lett.*, *7*, 41–44, doi:10.1029/GL007i001p00041.

Bagenal, F., D. E. Shemansky, R. L. McNutt Jr., R. Schreier, and A. Eviatar (1992), The abundance of $O^{++}$ in the Jovian magnetosphere, *Geophys. Res. Lett.*, *19*, 79–82, doi:10.1029/92GL00070.
Bagenal, F., et al. (2014), Magnetospheric Science Objectives of the Juno Mission, *Space Sci. Rev.*, doi:10.1007/s11214-014-0036-8.
Bagenal, F., E. Sidrow, R. J. Wilson, T. A. Cassidy, V. Dols, F. J. Crary, A. J. Steffl, P. A. Delamere, W. S. Kurth, and W. R. Paterson (2015), Plasma conditions at Europa's orbit, *Icarus*, *261*, 1–13.
Bagenal, F., R. J. Wilson, S. Siler, W. Paterson, and W. Kurth (2016), Survey of Galileo plasma observations in Jupiter's plasma sheet, *J. Geophys. Res. Planets*, *121*, 871–894, doi:10.1002/2016JE005009.
Bagenal, F., L. P. Dougherty, K. M. Bodisch, J. D. Richardson, and J. M. Belcher (2017), Survey of voyager plasma science ions I: Analysis method, *J. Geophys. Res. Planets*, *122*, doi:10.1002/2016JA023797.
Barbosa, D. D., and M. A. Moreno (1988), A comprehensive model of ion diffusion and charge exchange in the cold Io torus, *J. Geophys. Res.*, *93*, 823–836, doi:10.1029/JA093iA02p00823.
Barnett, A., and S. Olbert (1986), Response function of modulated grid faraday cup plasma instruments, *Rev. Sci. Instrum.*, *57*, 2432–2440, doi:10.1063/1.1139089.
Barnhart, B. L., W. S. Kurth, J. B. Groene, J. B. Faden, O. Santolik, and D. A. Gurnett (2009), Electron densities in Jupiter's outer magnetosphere determined from Voyager 1 and 2 plasma wave spectra, *J. Geophys. Res.*, *114*, A05218, doi:10.1029/2009JA014069.
Bodisch, K. M., L. P. Dougherty, and F. Bagenal (2017), Survey of Voyager plasma science ions at Jupiter: 3. Protons and minor ions, *J. Geophys. Res. Space Physics*, *122*, doi:10.1002/2017JA024148.
Bolton, S. J., R. M. Thorne, D. A. Gurnett, W. S. Kurth, and D. J. Williams (1997), Enhanced whistler-mode emissions: Signatures of interchange motion in the Io torus, *Geophys. Res. Lett.*, *24*, 2123–2126.
Bridge, H. S., J. W. Belcher, R. J. Butler, A. J. Lazarus, A. M. Mavretic, J. D. Sullivan, G. L. Siscoe, and V. M. Vasyliunas (1977), The plasma experiment on the 1977 Voyager mission, *Space Sci. Rev.*, *21*, 259–287.
Broadfoot, A. L., et al. (1979), Extreme ultraviolet observations from Voyager I encounter with Jupiter, *Science*, *204*, 979–982.
Brown, R. A., C. B. Pilcher, and D. F. Strobel (1983), *Physics of the Jovian Magnetosphere*, edited by A. J. Dessler, pp. 395–453, Cambridge Univ. Press, New York.
Brown, M. E. (1994), Observation of mass loading in the Io plasma torus, *Geophys. Res. Lett.*, *21*, 847–850.
Clark, G., B. H. Mauk, C. Paranicas, P. Kollmann, and H. T. Smith (2016), Charge states of energetic oxygen and sulfur ions in Jupiter's magnetosphere, *J. Geophys. Res. Planets*, *121*, 2264–2273, doi:10.1002/2015JA022257.
Connerney, J. E. P., M. H. Açuna, and N. F. Ness (1981), Modeling the Jovian current sheet and inner magnetosphere, *J. Geophys. Res.*, *86*, 8370–8384, doi:10.1029/JA086iA10p08370.
Connerney, J. E. P., M. H. Acuña, N. F. Ness, and T. Satoh (1998), New models of Jupiter's magnetic field constrained by the Io flux tube footprint, *J. Geophys. Res.*, *103*(A6), 11,929–11,939, doi:10.1029/97JA03726.
Connerney, J. E. P., et al. (2017), The Juno magnetic field investigation, *Space Sci. Rev.*, doi:10.1007/s11214-017-0334-z.
Crary, F. J., F. Bagenal, L. A. Frank, and W. R. Paterson (1998), Galileo plasma spectrometer measurements of composition and temperature in the Io plasma torus, *J. Geophys. Res.*, *103*, 29,359–29,370, doi:10.1029/1998JA900003.
Delamere, P. and F. Bagenal (2003), Modeling variability of plasma conditions in the Io torus. *J. Geophys. Res.*, *108*(A7), 1276, doi:10.1029/2002JA009706.
Delamere, P., A. Steffl, and F. Bagenal (2004), Modeling temporal variability of plasma conditions in the Io torus during the Cassini era, *J. Geophys. Res.*, *109*, A10216, doi:10.1029/2003JA010354.
Delamere, P., F. Bagenal, and A. Steffl (2005), Radial variations in the Io plasma torus during the Cassini era, *J. Geophys. Res.*, *110*, A12223, doi:10.1029/2005JA011251.
Dere, K. P., E. Landi, H. E. Mason, B. C. Monsignori Fossi, and P. R. Young (1997), CHIANTI—An atomic database for emission lines—Paper I: Wavelengths greater than 50 Å, *A&A Suppl. Ser.*, *125*, 149–173.
Esposito, L. W., et al. (2004), The Cassini ultraviolet imaging spectrograph, *Space Sci. Rev.*, *115*, 299–361.
Fazakerley, A. N., and D. J. Southwood (1992), Drift waves, magnetospheric interchange instability and plasma transport in the magnetosphere of Jupiter, *J. Geophys. Res.*, *97*, 10,787–10,800, doi:10.1029/92JA00280.
Fazakerley, A. N., and D. J. Southwood (1993), Magnetospheric interchange instability in anisotropic plasma, *Planet. Space Sci.*, *41*, 245–255.
Frank, L. A., and W. R. Paterson (2000a), Observations of plasmas in the Io torus with the Galileo spacecraft, *J. Geophys. Res.*, *105*, 16,017–16,034, doi:10.1029/1999JA000250.
Frank, L. A., and W. R. Paterson (2000b), Return to Io by the Galileo spacecraft: Plasma observations, *J. Geophys. Res.*, *105*, 25,363–25,378, doi:10.1029/1999JA000460.
Frank, L. A., and W. R. Paterson (2004), Plasmas observed near local noon in Jupiter's magnetosphere with the Galileo spacecraft, *J. Geophys. Res.*, *109*, A11217, doi:10.1029/2002JA009795.
Frank, L. A., W. R. Paterson, and K. K. Khurana (2002), Observations of thermal plasmas in Jupiter's magnetotail, *J. Geophys. Res.*, *107*(A1), 1003, doi:10.1029/2001JA000077.
Geiss, J., et al. (1992), Plasma composition in Jupiter's magnetosphere: Initial results from the solar wind ion composition spectrometer, *Science*, *257*, 1535.
Gustin, J., J.-C. G.rard, D. Grodent, S. W. H. Cowley, J. T. Clarke, and A. Grard (2004), Energy-flux relationship in the FUV Jovian aurora deduced from HST-STIS spectral observations, *J. Geophys. Res.*, *109*, A10205, doi:10.1029/2003JA010365.
Herbert, F., and B. R. Sandel (2000), Azimuthal variation of ion density and electron temperature in the Io plasma torus, *J. Geophys. Res.*, *105*, 16,035–16,052, doi:10.1029/1998JA000259.
Herbert, F., N. M. Schneider, and A. J. Dessler (2008), A new description of Io's cold plasma torus, *J. Geophys. Res.*, *113*, A01208, doi:10.1029/2007JA012555.
Hill, T. W. (1979), Inertial limit on corotation, *J. Geophys. Res.*, *84*, 6554–6558, doi:10.1029/JA084iA11p06554.
Hill, T. W. (1980), Corotation lag in Jupiter's magnetosphere—Comparison of observation and theory, *Science*, *207*, 301–302.
Huang, T. S., and T. W. Hill (1989), Corotation lag of the Jovian atmosphere, ionosphere, and magnetosphere, *J. Geophys. Res.*, *94*, 3761–3765, doi:10.1029/JA094iA04p03761.
Kivelson, M. G., and D. J. Southwood (2005), Dynamical consequences of two modes of centrifugal instability in Jupiter's outer magnetosphere, *J. Geophys. Res.*, *94*, A12209, doi:10.1029/2005JA011176.
Kivelson, M. G., K. K. Khurana, C. T. Russell, and R. J. Walker (1997), Intermittent short-duration magnetic field anomalies in the Io torus: Evidence for plasma interchange, *Geophys. Res. Lett.*, *24*, 2127–2130, doi:10.1029/97GL02202.
Krimigis, S. M., J. F. Carbary, E. P. Keath, C. O. Bostrom, W. I. Axford, G. Gloeckler, L. J. Lanzerotti, and T. P. Armstrong (1981), Characteristics of hot plasma in the Jovian magnetosphere: Results from the Voyager spacecraft, *J. Geophys. Res.*, *86*, 8227–8257, doi:10.1029/JA086iA10p08227.

Hamilton, D. C., G. Gloeckler, S. M. Krimigis, and L. J. Lanzerotti (1981), Composition of nonthermal ions at the Jovian magnetosphere, *J. Geophys. Res.*, *86*, 8301–8318, doi:10.1029/JA086iA10p08301.
Lanzerotti, L. J., C. G. Maclennan, and D. M. Feldman (1993), Ulysses measurements of energetic H3 molecules in Jupiter's magnetosphere, *J. Geophys. Res.*, *98*, 21,145–21,149.
Maclennan, C. G., L. J. Lanzerotti, and A. Lagg (2001), Hot plasma heavy ion abundance in the inner Jovian magnetosphere (<10 Rj), *Planet. Space Sci.*, *49*, 275–282.
Mauk, B. H., S. A. Gary, M. Kane, E. P. Keath, and S. M. Krimigis (1996), Hot plasma parameters of Jupiter's inner magnetosphere, *J. Geophys. Res.*, *101*, 7685–7695, doi:10.1029/96JA00006.
Mauk, B. H., D. J. Williams, R. W. McEntire, K. K. Khurana, and J. G. Roederer (1999), Storm-like dynamics of Jupiter's inner and middle magnetosphere, *J. Geophys. Res.*, *104*, 22,759–22,778, doi:10.1029/1999JA900097.
Mauk, B. H., D. G. Mitchell, R. W. McEntire, C. P. Paranicas, E. C. Roelof, D. J. Williams, and S. M. Krimigis (2001), Energetic ion characteristics and neutral gas interactions in Jupiter's magnetosphere, *J. Geophys. Res.*, *109*, doi:10.1029/2003JA010270.
McNutt, R. L., Jr., J. W. Blecher, J. D. Sullivan, F. Bagenal, and H. S. Bridge (1979), Departure from rigid co-rotation of plasma in Jupiter's dayside magnetosphere, *Nature*, *280*, 803.
McNutt, R. L., Jr., J. W. Belcher, and S. H. Bridge (1981), Positive ion observations in the middle magnetosphere of Jupiter, *J. Geophys. Res.*, *86*, 8319–8342, doi:10.1029/JA086iA10p08319.
McNutt, R. L., Jr., P. S. Coppi, R. S. Selesnick, and B. Coppi (1987), Plasma depletions in the Jovian magnetosphere: Evidence of transport and solar wind interaction, *J. Geophys. Res.*, *92*, 4377–4398, doi:10.1029/JA092iA05p04377.
Nerney, E., F. Bagenal, and A. Steffl (2017), Io plasma torus ion composition: Voyager, Galileo, Cassini, *J. Geophys. Res. Planets*, *122*, 727–744, doi:10.1002/2016JA023306.
Nichols, J. D., and S. W. H. Cowley (2004), Magnetosphere-ionosphere coupling currents in Jupiter's middle magnetosphere: Effect of precipitation-induced enhancement of the ionospheric Pedersen conductivity, *Ann. Geophys.*, *22*, 1799–1827, doi:10.5194/angeo-22-1799-2004.
Phillips, J. l., S. J. Bame, B. L. Barraclough, D. J. McComas, R. J. Forsyth, P. Canuj, and P. J. Kellogg (1993), Uysses plasma electron observations in the Jovian magnetosphere, *Planet. Space Sci.*, *41*, 877–892.
Pontius, D. H. (1995), Implications of variable mass loading in the Io torus: The Jovian flywheel, *J. Geophys. Res.*, *100*, 19,531–19,540, doi:10.1029/95JA01554.
Pontius, D. H., Jr., T. W. Hill, and M. E. Rassbach (1986), Steady state plasma transport in a corotation dominated magnetosphere, *Geophys. Res. Letts.*, *11*, 1097–1100, doi:10.1029/GL013i011p01097.
Pontius, D. H., Jr., R. A. Wolf, T. W. Hill, R. W. Spiro, Y. S. Yang, and W. H. Smyth (1998), Velocity shear impoundment of the Io plasma torus, *J. Geophys. Res.*, *103*, 19,935–19,946, doi:10.1029/98JE00538.
Ray, L. C., R. E. Ergun, P. A. Delamere, and F. Bagenal (2010), Magnetosphere-ionosphere coupling at Jupiter: Effect of field-aligned potentials on angular momentum transport, *J. Geophys. Res.*, *115*, A09211, doi:10.1029/2010JA015423.
Ray, L. C., R. E. Ergun, P. A. Delamere, and F. Bagenal (2012), Magnetosphere-ionosphere coupling at Jupiter: A parameter space study, *J. Geophys. Res.*, *117*, A01205, doi:10.1029/2011JA016899.
Ray, L. C., N. A. Achilleos, M. F. Vogt, and J. N. Yates (2014), Local time variations in Jupiter's magnetosphere-ionosphere coupling system, *J. Geophys. Res. Space Physics*, *119*, 4740–4751, doi:10.1002/2014JA019941.
Ray, L. C., N. A. Achilleos, and J. N. Yates (2015), The effect of including field-aligned potentials in the coupling between Jupiter's thermosphere, ionosphere, and magnetosphere, *J. Geophys. Res. Planets*, *120*, 6987–7005, doi:10.1002/2015JA021319.
Richardson, J. D., and R. L. McNutt Jr. (1987), Observational constraints on interchange models at Jupiter, *Geophys. Res. Lett.*, *14*, 64–67, doi:10.1029/GL014i001p00064.
Richardson, J. D., and G. L. Siscoe (1983), The problem of cooling the cold Io torus, *J. Geophys. Res.*, *88*, 2001–2009, doi:10.1029/JA088iA03p02001.
Richardson, J. D., G. L. Siscoe, F. Bagenal, and J. D. Sullivan (1980), Time dependent plasma injection by Io, *Geophys. Res. Lett.*, *7*, 37–40, doi:10.1029/GL007i001p00037.
Russell, C. T., M. G. Kivelson, and K. K. Khurana (2005), Statistics of depleted flux tubes in the Jovian magnetosphere, *Planet. Space Sci.*, *53*, 937–943.
Sandel, B. R., and A. J. Dessler (1988), Dual periodicity of the Jovian magnetosphere, *J. Geophys. Res.*, *93*, 5487–5504, doi:10.1029/JA093iA06p05487.
Sandel, B. R., et al. (1979), Extreme ultraviolet observations from Voyager 2 encounter with Jupiter, *Science*, *206*, 962–966.
Sands, M. R., and R. L. McNutt Jr. (1988), Plasma bulk flow in Jupiter's dayside middle magnetosphere, *J. Geophys. Res.*, *93*, 8502–8518, doi:10.1029/JA093iA08p08502.
Schneider, N. M., and F. Bagenal (2007), Io's neutral clouds, plasma torus, and magnetospheric interaction, in *Io After Galileo*, edited by R. C. Lopes and J. R. Spencer, pp. 265–286, Springer, New York.
Scudder, J. D., E. C. Sittler Jr., and H. S. Bridge (1981), A survey of the plasma electron environment of Jupiter: A view from Voyager, *J. Geophys. Res.*, *86*, 8157–8179, doi:10.1029/JA086iA10p08157.
Siscoe, G. L. (1978), Jovian plasmaspheres, *J. Geophys. Res.*, *83*, 2118–2126, doi:10.1029/JA083iA05p02118.
Siscoe, G. L., and C.-K. Chen (1977), Io: A source for Jupiter's inner plasmasphere, *Icarus*, *31*, 1–10.
Siscoe, G. L., and D. Summers (1981), Centrifugally driven diffusion of iogenic plasma, *J. Geophys. Res.*, *86*, 8471–8479, doi:10.1029/JA086iA10p08471.
Sittler, E. C., Jr., and D. F. Strobel (1987), Io plasma torus electrons: Voyager 1, *J. Geophys. Res.*, *92*, 5741–5762, doi:10.1029/JA092iA06p05741.
Shemansky, D. E. (1987), Ratio of oxygen to sulfur in the Io plasma torus, *J. Geophys. Res.*, *92*, 6141–6146, doi:10.1029/JA092iA06p06141.
Shemansky, D. E. (1988), Energy branching in the Io plasma torus: The failure of neutral cloud theory, *J. Geophys. Res.*, *93*, 1773–1784, doi:10.1029/JA093iA03p01773.
Smith, C. G. A., and A. D. Aylward (2009), Coupled rotational dynamics of Jupiter's thermosphere and magnetosphere, *Ann. Geophys.*, *27*, 199–230.
Steffl, A. J., F. Bagenal, and A. I. F. Stewart (2004a), Cassini UVIS observations of the Io plasma torus: I. Initial results, *Icarus*, *172*, 78–90.
Steffl, A. J., F. Bagenal, and A. I. F. Stewart (2004b), Cassini UVIS observations of the Io plasma torus: II. Radial variations, *Icarus*, *172*, 91–103.
Steffl, A. J., P. A. Delamere, and F. Bagenal (2006), Cassini UVIS observations of the Io plasma torus: III. Observations of temporal and azimuthal variability, *Icarus*, *180*, 124–140.
Steffl, A. J., P. A. Delamere, and F. Bagenal (2008), Cassini UVIS observations of the Io plasma torus: IV. Modeling temporal and azimuthal variability, *Icarus*, *194*(2008), 153–165.

Summers, D., and G. L. Siscoe (1985), Wave modes of the Io plasma torus, *Astrophys. J.*, *295*, 678–684.
Summers, D., and G. L. Siscoe (1986), A model of the Io plasma ribbon, *Icarus*, *67*, 520–524.
Thomas, N., G. Lichtenberg, and M. Scotto (2001), High-resolution spectroscopy of the Io plasma torus during the Galileo mission, *J. Geophys. Res.*, *106*, 26,277–26,291, doi:10.1029/2000JA002504.
Thomas, N., F. Bagenal, T. Hill, and J. Wilson (2004), The Io neutral clouds and plasma torus, in *Jupiter: Planet*, *Satellites*, *Magnetosphere*, edited by F. Bagenal, T. E. Dowling, and W. B. McKinnon, Cambridge Univ. Press, Cambridge, U. K.
Thorne, R. M., S. J. Bolton, T. P. Armstrong, D. A. Gurnett, M. G. Kivelson, R. W. McEntire, A. Roux, and D. J. Williams (1997), Galileo evidence for rapid interchange transport in the Io torus, *Geophys. Res. Lett.*, *24*, 2131–2134, doi:10.1029/97GL01788.
Vasyliunas, V. M. (1989), Maximum scales for preserving flux tube content in radial diffusion driven by interchange motions, *Geophys. Res. Lett.*, *16*, 1465–1468, doi:10.1029/GL016i012p01465.
Vogt, R. E., A. C. Cummings, T. L. Garrard, N. Gehrels, E. C. Stone, J. H. Trainor, A. W. Schardt, T. F. Cordon, and F. B. McDonald (1979a), Voyager 2: Energetic ions and electrons in the Jovian magnetosphere, *Science*, *206*, 984.
Vogt, R. E., et al. (1979b), Voyager 1: Energetic ions and electrons in the Jovian magnetosphere, *Science*, *204*, 1003.
Volwerk, M. (1997), Systems III and IV modulation of the Io phase effect in the Io plasma torus, *J. Geophys. Res.*, *102*, 24,403–224,41, doi:10.1029/97JA02368.
Volwerk, M., M. E. Brown, A. J. Dessler, and B. R. Sandel (1997), Evidence for short cooling time in the Io plasma torus, *Geophys. Res. Lett.*, *24*, 1147–1150, doi:10.1029/97GL00966.
Yang, Y. S., R. A. Wolf, R. W. Spiro, and A. J. Dessler (1992), Numerical simulation of plasma transport driven by the Io torus, *Geophys. Res. Lett.*, *19*, 957–960, doi:10.1029/92GL01031.
Yang, Y. S., R. A. Wolf, R. W. Spiro, T. W. Hill, and A. J. Dessler (1994), Numerical simulation of torus-driven plasma transport in the Jovian magnetosphere, *J. Geophys. Res.*, *99*, 8755–8770, doi:10.1029/94JA00142.